Applied Physics Letters

Skyrmion motion induced by voltage-controlled in-plane strain gradients

Cite as: Appl. Phys. Lett. **115**, 132401 (2019); https://doi.org/10.1063/1.5119085
Submitted: 08 July 2019 . Accepted: 06 September 2019 . Published Online: 23 September 2019

R. Yanes, F. Garcia-Sanchez, R. F. Luis, E. Martinez, V. Raposo, L. Torres, and L. Lopez-Diaz

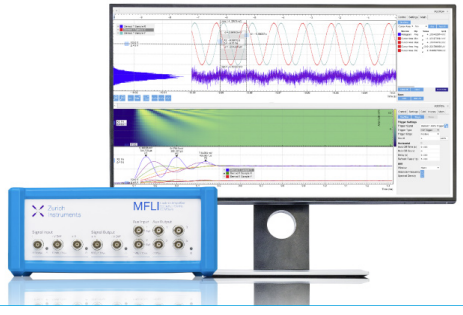

Applied Physics Letters ARTICLE scitation.org/journal/apl

Skyrmion motion induced by voltage-controlled in-plane strain gradients

Cite as: Appl. Phys. Lett. **115**, 132401 (2019); doi: 10.1063/1.5119085
Submitted: 8 July 2019 · Accepted: 6 September 2019 ·
Published Online: 23 September 2019

R. Yanes,[a] F. Garcia-Sanchez, R. F. Luis, E. Martinez, V. Raposo, L. Torres, and L. Lopez-Diaz

AFFILIATIONS

Department of Applied Physics, University of Salamanca, 37008 Salamanca, Spain

[a]ryanes@usal.es

ABSTRACT

Micromagnetic simulations are used to investigate the motion of magnetic skyrmions in an in-plane strain gradient. The skyrmion diameter and energy are found to depend on the strain, which leads to a force that moves the skyrmion toward regions with higher strain. An analytical expression for the skyrmion velocity as a function of the strain gradient is derived assuming a rigid profile for the skyrmion, and good agreement with simulations is obtained. Furthermore, electromechanical simulations of a hybrid ferromagnetic/piezoelectric device show that the in-plane strain gradients needed to move skyrmions can be achieved by applying moderate voltages in the piezoelectric substrate, which offers an original way to control skyrmion motion efficiently.

Magnetic skyrmions are chiral spin textures[1–3] that display promising features for use as future information carriers, such as small size, high stability, and possibility of easy confinement.[4–7] The ability to efficiently nucleate and control skyrmion motion is a key point in the development of future spintronic devices.[8,9]

The traditional way to move skyrmions is by spin-polarized currents,[10–13] but other approaches that do not involve charge currents and the associated Joule heating effects are being explored, such as electric fields,[14,15] spatially variable magnetic fields,[16,17] temperature gradients,[18,19] spin waves,[20] and voltage-controlled anisotropy gradients.[21–24]

Meanwhile, the possibility of controlling magnetic textures using mechanical stress is currently being investigated, with promising results in domain walls[25,26] and skyrmions.[27–31] In particular, there is experimental evidence that skyrmions can be nucleated and annihilated through stress control of the topological phase transition in bulk single crystals,[27,28] whereas simulations indicate that voltage-controlled strain-mediated switching of skyrmions is possible in heterostructures with the interfacial Dzyaloshinskii–Moriya (DM) interaction on top of a piezoelectric (PZ) substrate.[30,31] Simulations have also shown that vertical voltage-controlled strain pulses can be used to pin skyrmions.[30]

In this work, we combine electromechanical and micromagnetic simulations to explore a promising way to manipulate skyrmions using voltage-controlled strain. While previous studies have focused on nucleating, annihilating, and pinning skyrmions using this technique, we propose to use it as the sole mechanism that drives skyrmions in a given direction. In particular, we show that voltage-induced in-plane strain gradients create a net force on the skyrmions, which drives them toward regions with higher strain.

As shown schematically in Fig. 1(a), the proposed device consists of a ferromagnetic (FM) nanostripe deposited on a PZ substrate, with an Au electrode at each end. To avoid an electrical current through the FM layer, an air gap of 1 nm is imposed between the electrodes and the FM layer. We use COMSOL Multiphysics[32] to obtain the electromechanical response of the system when a certain voltage is applied. The profile along the x axis of ε_{xx}, the dominant component of the strain tensor, in the FM is plotted in Fig. 1(b), where a voltage of $V_0 = \pm 2$ V is applied between the electrodes, which are separated by a distance of $L_x = 400$ nm. A standard PZ substrate (namely, lead zirconate titanate PZ-4[32]) and typical parameter values for CoFeB (namely, $C_{11} = 218$ GPa, $C_{12} = 93$ GPa,[31] a Young's modulus of 162 GPa,[33] and a Poisson's ratio of $\nu = 0.3$) were used for the simulation. As can be observed, because of the inverse PZ effect, the voltage between the Au electrodes induces an inhomogeneous planar strain in the PZ layer that is partially transmitted to the FM. The strain is stronger close to the electrodes but decreases away from them, varying linearly in the central region of the FM nanostripe. More details about the electromechanical response of the system can be found in Sec. S1 of the supplementary material. In particular, we present a study on how the strain profile is affected by (i) the distance between the electrodes, (ii) the applied voltage, and (iii) the lateral confinement of the PZ layer. The results show that the strain profile is easily tailored to fit one's demands.

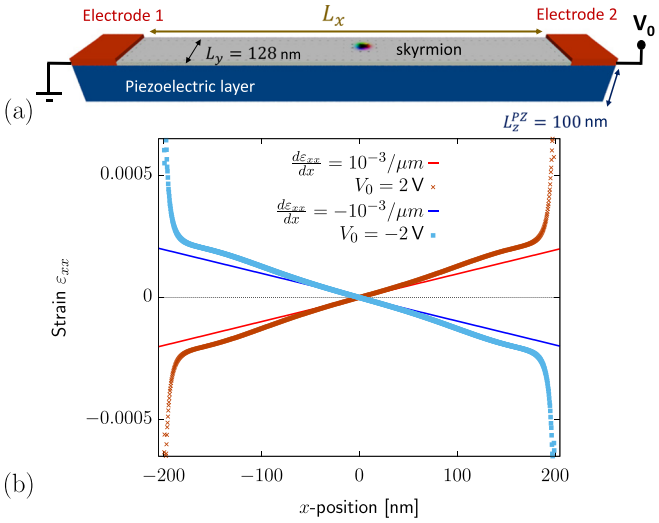

FIG. 1. (a) Sketch of the ferromagnetic/piezoelectric (FM/PZ) heterostructure under study. (b) Profile of strain ε_{xx} along the centerline (x axis) of the FM nanostripe for $L_x = 400$ nm and $V_0 = \pm 2$ V. The symbols are the results obtained using COMSOL Multiphysics,[32] while the solid lines are the linear profiles used in the micromagnetic simulations, namely, $\frac{d\varepsilon_{xx}}{dx} = \pm 10^{-3}\ \mu\text{m}^{-1}$.

In what follows, we investigate the effect that a strain profile like to the one shown in Fig. 1(b) has on a skyrmion stabilized in the FM layer. To do so, we solve the Landau–Lifshitz–Gilbert equation[34] numerically. With exchange, magnetocrystalline anisotropy, magnetostatic, and interfacial DM contributions, we include a magnetoelastic field given by[35,36]

$$\vec{H}_{me} = \frac{1}{\mu_0 M_s}\hat{\boldsymbol{\sigma}}\cdot\frac{\partial\hat{\boldsymbol{\varepsilon}}^m}{\partial\vec{m}}, \tag{1}$$

where $\hat{\boldsymbol{\sigma}}$ and $\hat{\boldsymbol{\varepsilon}}^m$ are the stress and magnetic strain tensors, respectively, M_s is the saturation magnetization, and $\vec{m}$ is the normalized magnetization. Micromagnetic simulations were performed using the GPU-based software package mumax[3] (Ref. 37) modified to include the magnetoelastic contribution from a spatially dependent strain.

We consider a thin magnetic film of dimensions $L_x = 1024$ nm, $L_y = 128$ nm, and $L_z = 1$ nm with values of the magnetic and elastic material parameters that are typical for oxide/$Co_{20}Fe_{60}B_{20}$/heavy metal, namely, an exchange constant of $A_{ex} = 1.9 \times 10^{-11}$ J/m, $M_s = 1.0 \times 10^6$ A/m, an anisotropy constant of $K = 8.0 \times 10^5$ J/m^3,[38] a DM constant of $D = 1.8$ mJ/m^2, a damping parameter of $\alpha = 0.015$, elastic constants of $C_{11} = 218$ GPa and $C_{12} = 93$ GPa, and a magnetostriction parameter of $\lambda_s = 3.7 \times 10^{-5}$.[31] We choose this material because at this thickness, CoFeB is magnetized perpendicularly,[39] displays a phase diagram capable of sustaining skyrmions,[30,40,41] and exhibits a significant elastic response.[31]

For our theoretical study, we impose a Néel skyrmion at the center of the nanostripe. Were the device to be fabricated, a mechanism to nucleate skyrmions in a controllable manner would be necessary. Among the different approaches explored theoretically,[11,31] we would be inclined to nucleate the skyrmion with perpendicular strain because this would mean a fully voltage-controlled device. This would require a third electrode below the PZ substrate and some geometrical modifications that favor skyrmion nucleation. However, these details are beyond the present scope, and here, we investigate skyrmion dynamics under the effect of a strain gradient.

For simplicity, we consider only the strain ε_{xx} along the x axis and assume that it varies linearly with x. Electromechanical simulations also give a small transverse strain ε_{yy}, but this contribution can be tuned with the lateral dimension of the PZ layer (see Sec. S1 of the supplementary material).

Assuming that CoFeB is isotropic and that ε_{xx} is the only nonzero component of the strain tensor, the magnetoelastic field can be written as

$$\begin{aligned} H_{me}^x &\approx \frac{3\lambda_s}{\mu_0 M_s} C_{11}\varepsilon_{xx} m_x, \\ H_{me}^y &\approx \frac{3\lambda_s}{\mu_0 M_s} C_{12}\varepsilon_{xx} m_y. \end{aligned} \tag{2}$$

Consequently, a uniaxial longitudinal strain gradient leads to an inhomogeneous in-plane magnetoelastic field that depends on the magnetization. The derivation of Eq. (2) from the general linear elastic and magnetoelastic constitutive relations is presented in Sec. S2 of the supplementary material.

Figure 2 shows snapshots of the magnetization configuration at three time instants $t = 0.5$, 20, and 40 ns corresponding to either a positive (right) or negative (left) strain gradient of modulus $\frac{d\varepsilon_{xx}}{dx} = 10^{-3}\ \mu\text{m}^{-1}$. These results imply that skyrmions move in the direction in which the strain increases, which, as shown before, can be controlled with the sign of the applied voltage [see Fig. 1(b)].

Looking at the dynamics in detail, we observe that because of the skyrmion Hall effect,[11,41] initially, the skyrmion moves obliquely with $v_y > v_x$, but the repulsive effect from the border gradually compensates for v_y until a steady velocity in the x direction ($v_y = 0$) is eventually reached (see the animation in Sec. S6 of the supplementary material). This steady velocity v_x is computed for different values of the strain gradient, and the results are presented in Fig. 3. As can be seen, the velocity depends linearly on the strain slope, which in turn depends linearly on the applied voltage (see Sec. S1 of the supplementary material).

To understand the origin of this strain-induced skyrmion motion, we investigate how the skyrmion energy E_{sk} and diameter d_{sk} depend on the strain. This is shown in Fig. 4, for which E_{sk} and d_{sk} were evaluated numerically, assuming a uniform strain in the nanostripe and a skyrmion at the center. As can be seen, the diameter increases with strain, whereas the energy decreases. This tells us that longitudinal strain helps to stabilize skyrmions, and it explains why they move in the direction of increasing strain. The results in Fig. 4 can be understood qualitatively if we consider that, as shown before, the effect of ε_{xx} on the magnetization is equivalent to an in-plane field whose longitudinal (H_{me}^x) and transverse (H_{me}^y) components are

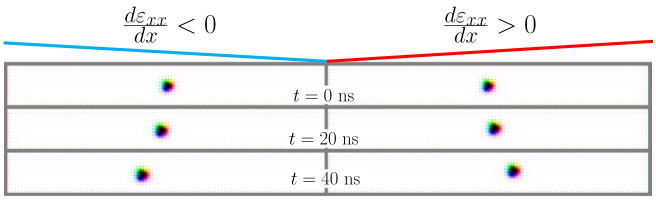

FIG. 2. Snapshots of magnetization $\vec{m}$ (plotted on the color scale) under the effect of a uniform stress gradient $\frac{d\varepsilon_{xx}}{dx} = -10^{-3}\ \mu\text{m}^{-1}$ (left) and $10^{-3}\ \mu\text{m}^{-1}$ (right) for three time instants $t = 0$, 20, and 40 ns. The solid lines indicate the x-dependence of the strain ε_{xx}.

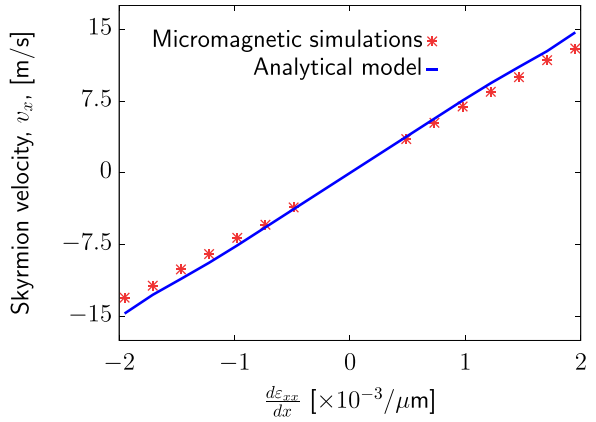

FIG. 3. Skyrmion steady velocity, v_x, as a function of the strain slope. The symbols are the results from micromagnetic simulations, while the line corresponds to the analytical model of Eq. (9).

proportional to m_x and m_y, respectively [see Eq. (2)]. This field acts mainly in the skyrmion wall, where the magnetization lies in the plane.

The inset of Fig. 4 shows a schematic of the skyrmion and $\vec{H}_{me}$ at different points on the skyrmion wall. $\vec{H}_{me}$ is predominantly parallel to the magnetization over the wall, thereby increasing the skyrmion diameter and decreasing its energy. This simple representation also explains the origin of the force that moves the skyrmions along the strain gradient. $\vec{H}_{me}$ is proportional to the strain and, in the presence of a strain gradient, is no longer symmetric with respect to the skyrmion center but rather is larger (respectively, smaller) on the side where the strain is higher (respectively, smaller), which leads to a net force along the strain gradient.

We have developed a Thiele model to investigate strain-induced skyrmion motion further. Assuming that the skyrmion moves rigidly, the equation of motion can be written as[42]

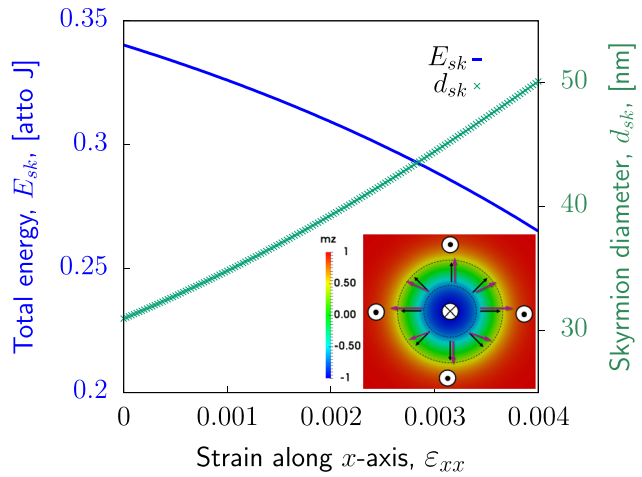

FIG. 4. Skyrmion diameter d_{sk} and energy E_{sk} as functions of the strain. E_{sk} is calculated as the difference between the energy of the system with the skyrmion at the center and the saturated ferromagnetic state. Inset: skyrmion with the sketch of both magnetization (black arrows) and magnetoelastic fields (pink arrows) at different points on the skyrmion wall (green area).

$$\mathbf{G}\times\mathbf{v}-\alpha\hat{\mathbf{D}}\mathbf{v}+\mathbf{F}=0, \tag{3}$$

where $\mathbf{G}=-\frac{4\pi N_{sk}L_zM_s}{\gamma}\mathbf{k}=G\mathbf{k}$ is the gyrovector, N_{sk} is the skyrmion number ($N_{sk}=-1$ for our Néel skyrmion), $\hat{\mathbf{D}}=\frac{M_s}{\gamma}\int_v\mathbf{m}\left(\frac{d\mathbf{m}}{dx_i}\times\frac{d\mathbf{m}}{dx_j}\right)dV$ is the dissipation tensor, and $\mathbf{F}=-M_s\int_v\mathbf{H}_{me}\frac{d\mathbf{m}}{d\mathbf{x}}dV$ is the force on the skyrmion.

The following ansatz is chosen for the magnetization profile $\vec{m}=(\sin\Theta\cos\varphi,\ \sin\Theta\sin\varphi,\ \cos\Theta)$:

$$\Theta=\begin{cases}\frac{\pi}{\Delta}(\Delta-r), & 0\le r\le\Delta,\\ 0, & r>\Delta,\end{cases} \tag{4}$$

where $(r,\ \varphi)$ are the in-plane polar coordinates $[X=r\cos(\varphi),\ Y=r\sin\varphi]$ and Δ is the width of the skyrmion wall. As shown in Sec. S3 of the supplementary material, this ansatz corresponds to a zero-radius skyrmion, fits reasonably to the profile computed numerically, and allows us to obtain analytical expressions for $\hat{\mathbf{D}}$ and $\mathbf{F}$.

With our symmetric ansatz of Eq. (4), we obtain $D_{xy}=D_{yx}=0$ and $D_{xx}=D_{yy}=\mathcal{D}$ with

$$\mathcal{D}=\frac{\pi M_sL_z}{2\gamma}\left(\pi^2-\mathrm{Ci}(2\pi)+\gamma_E+\log(2\pi)\right), \tag{5}$$

where Ci is the cosine integral function and γ_E Euler's constant. Interestingly, $\mathcal{D}$ is not affected by the strain. Meanwhile, for the force, we obtain

$$F_x=\frac{3\pi\Delta^2\lambda_sL_z}{8\mu_0}(C_{11}+C_{12})\frac{d\varepsilon_{xx}}{dx}. \tag{6}$$

According to Eq. (3), the general solution for the skyrmion's velocity is

$$\begin{pmatrix}v_x\\ v_y\end{pmatrix}=\frac{1}{\alpha^2\mathcal{D}^2+G^2}\begin{pmatrix}\alpha\mathcal{D}F_x-F_yG\\ \alpha\mathcal{D}F_y+F_xG\end{pmatrix}, \tag{7}$$

where in addition to F_x [Eq. (6)], we consider F_y due to the boundary repulsion.[22,41,43,44]

Initially, the skyrmion is located far from the borders and does not experience repulsion ($F_y=0$). Thus, the velocity can then be approximated by

$$\begin{pmatrix}v_x\\ v_y\end{pmatrix}\simeq\frac{1}{\alpha^2\mathcal{D}^2+G^2}\begin{pmatrix}\alpha\mathcal{D}F_x\\ F_xG\end{pmatrix}, \tag{8}$$

so that the skyrmion moves obliquely in a direction ϕ given by $\tan\phi=v_y/v_x=G/(\alpha\mathcal{D})$.[41]

As the skyrmion approaches a boundary, F_y increases until it balances the gyrotropic contribution of F_x. When this condition is reached, we have $v_y=0$, and the skyrmion moves in the x direction with a steady velocity given by

$$v_x=\frac{F_x}{\alpha\mathcal{D}}. \tag{9}$$

Therefore, our model predicts that the skyrmion velocity depends linearly on the strain slope and also on the skyrmion's area ($\propto\Delta^2$). The velocity dependence on the strain gradient that our model predicts [Eqs. (6) and (9)] is shown in Fig. 3 (solid line), showing good quantitative agreement with the results of micromagnetic simulations.

The value of Δ used in the model was obtained by fitting the skyrmion profile at $\varepsilon_{xx} = 0$ to the ansatz of Eq. (4), giving $\Delta = 30.4$ nm. Note that a discrepancy between the model and the simulations becomes apparent for large strain gradients. One should remember that for large strain gradients, the skyrmion reaches its steady velocity close to the boundary (see the animations in the supplementary material), in which case the repulsive force in the x direction, which is not taken into account in our model, becomes relevant and modifies the skyrmion trajectory, leading to a reduction of v_x.

As a final test for the efficiency of our scheme, we compare it with the traditional way of moving skyrmions, namely, by passing a current through the adjacent heavy-metal layer. The results are presented in Fig. 5, where the steady velocities for different values of the strain gradient and current density J are plotted for the strain-driven and current-driven schemes, respectively. The same sample dimensions and material parameters as specified earlier in the text were used in both cases, whereas a spin Hall coefficient of $\theta_{SH} = -0.33$ was used for the current-driven simulations;[45,46] see Sec. S5 of the supplementary material for more details. From Fig. 5, we conclude that a strain gradient of the order of $10^{-3}\,\mu\text{m}^{-1}$ results in a skyrmion velocity similar to that obtained by passing a current of the order of 10^9 A/m^2. As shown in Fig. 1 and Sec. S1 of the supplementary material, we note that such strain gradients can be obtained by applying moderate voltages (a few volts) in the PZ substrate. According to our calculations, the energy required to move the skyrmion between the two contacts is of the same order for the two methods. However, it should be noted that for the current-driven method, the energy is dissipated via Joule heating, whereas in the strain-gradient method, the energy is restored to the battery when the voltage is switched off.

In summary, we have proposed a scheme to move skyrmions based on creating an in-plane strain gradient that, via magnetoelastic coupling, creates a force that drives the skyrmions in the direction of increasing strain with a velocity that depends linearly on the strain gradient. Moreover, we proposed a device to implement this scheme, in which a magnetic nanostripe is deposited on a PZ substrate and the strain gradient is created by applying a voltage between electrodes located at each end of the device. Electromechanical simulations showed that the strain gradients required to move skyrmions can be achieved by applying moderate voltages. Although there is room for optimization, such as by exploring additional strain contributions (see Sec. S4 of the supplementary material), overall, our scheme has the attractive features of reversibility, robustness, and scalability. Most importantly, it is voltage controlled and involves no charge current or magnetic field, thereby making it suitable for developing environmentally friendly spintronic devices.

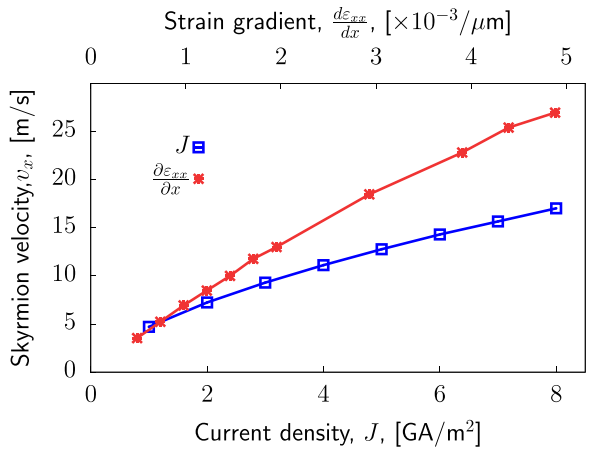

FIG. 5. Steady skyrmion speed as a function of either current density (blue, $\theta_{SH} = -0.33$) or strain gradient (red).

See the supplementary material for (i) the electromechanical simulation, (ii) details of the elastic magnetoelastic model, (iii) the ansatz for the skyrmion profile, (iv) comments on other contributions of the strain tensor, (v) details of the equations for the magnetization dynamics, and (vi) animations of the skyrmion's motion.

This work was supported by Project No. MAT2017-87072-C4-1-P from the (Ministerio de Economía y Competitividad) Spanish government and Project No. SA299P18 from Consejería de Educación Junta de Castilla y León.

REFERENCES

[1]A. Bogdanov and A. Hubert, J. Magn. Magn. Mater. **138**, 255 (1994).
[2]U. K. Röß ler, A. N. Bogdanov, and C. Pfleiderer, Nature **442**, 797 (2006).
[3]S. Mühlbauer, B. Binz, F. Jonietz, C. Pfleiderer, A. Rosch, A. Neubauer, R. Georgii, and P. Böni, Science **323**, 915 (2009).
[4]A. Fert, V. Cros, and J. Sampaio, Nat. Nanotechnol. **8**, 152 (2013).
[5]N. Nagaosa and Y. Tokura, Nat. Nanotechnol. **8**, 899 (2013).
[6]A. O. Leonov, T. L. Monchesky, N. Romming, A. Kubetzka, A. N. Bogdanov, and R. Wiesendanger, New J. Phys. **18**, 065003 (2016).
[7]K. Everschor-Sitte, J. Masell, R. M. Reeve, and M. Kläui, J. Appl. Phys. **124**, 240901 (2018).
[8]A. Fert, N. Reyren, and V. Cros, Nat. Rev. Mater. **2**, 17031 (2017).
[9]X. Zhang, Y. Zhou, K. M. Song, T.-E. Park, J. Xia, M. Ezawa, X. Liu, W. Zhao, G. Zhao, and S. Woo, preprint arXiv:1906.04718 (2019).
[10]F. Jonietz, S. Mühlbauer, C. Pfleiderer, A. Neubauer, W. Münzer, A. Bauer, T. Adams, R. Georgii, P. Böni, R. A. Duine, K. Everschor, M. Garst, and A. Rosch, Science **330**, 1648 (2010).
[11]J. Sampaio, V. Cros, S. Rohart, A. Thiaville, and A. Fert, Nat. Nanotechnol. **8**, 839 (2013).
[12]S. Woo, K. Litzius, B. Krüger, M.-Y. Im, L. Caretta, K. Richter, M. Mann, A. Krone, R. M. Reeve, M. Weigand, P. Agrawal, I. Lemesh, M.-A. Mawass, P. Fischer, M. Kläui, and G. S. D. Beach, Nat. Mater. **15**, 501 (2016).
[13]W. Legrand, D. Maccariello, N. Reyren, K. Garcia, C. Moutafis, C. Moreau-Luchaire, S. Collin, K. Bouzehouane, V. Cros, and A. Fert, Nano Lett. **17**, 2703 (2017).
[14]P. Upadhyaya, G. Yu, P. K. Amiri, and K. L. Wang, Phys. Rev. B **92**, 134411 (2015).
[15]C. Ma, X. Zhang, J. Xia, M. Ezawa, W. Jiang, T. Ono, S. N. Piramanayagam, A. Morisako, Y. Zhou, and X. Liu, Nano Lett. **19**, 353 (2019).
[16]C. Wang, D. Xiao, X. Chen, Y. Zhou, and Y. Liu, New J. Phys. **19**, 083008 (2017).
[17]F. Büttner, C. Moutafis, M. Schneider, B. Krüger, C. M. Günther, J. Geilhufe, C. V. K. Schmising, J. Mohanty, B. Pfau, S. Schaffert, A. Bisig, M. Foerster, T. Schulz, C. A. F. Vaz, J. H. Franken, H. J. M. Swagten, M. Kläui, and S. Eisebitt, Nat. Phys. **11**, 225 (2015).
[18]L. Kong and J. Zang, Phys. Rev. Lett. **111**, 067203 (2013).
[19]S.-Z. Lin, C. D. Batista, C. Reichhardt, and A. Saxena, Phys. Rev. Lett. **112**, 187203 (2014).
[20]G. Zhang, Y. Tian, Y. Deng, D. Jiang, and S. Deng, J. Nanotechnol. **2018**, 2602913.
[21]W. Kang, Y. Huang, C. Zheng, W. Lv, N. Lei, Y. Zhang, X. Zhang, Y. Zhou, and W. Zhao, Sci. Rep. **6**, 23164 (2016).

[22]X. Wang, W. L. Gan, J. C. Martinez, F. N. Tan, M. B. A. Jalil, and W. S. Lew, Nanoscale **10**, 733 (2018).
[23]R. Tomasello, S. Komineas, G. Siracusano, M. Carpentieri, and G. Finocchio, Phys. Rev. B **98**, 024421 (2018).
[24]Y. Liu, N. Lei, C. Wang, X. Zhang, W. Kang, D. Zhu, Y. Zhou, X. Liu, Y. Zhang, and W. Zhao, Phys. Rev. Appl. **11**, 014004 (2019).
[25]N. Lei, T. Devolder, G. Agnus, P. Aubert, L. Daniel, J.-V. Kim, W. Zhao, T. Trypiniotis, R. P. Cowburn, C. Chappert, D. Ravelosona, and P. Lecoeur, Nat. Commun. **4**, 1378 (2013).
[26]V. Sampath, N. D'Souza, G. M. Atkinson, S. Bandyopadhyay, and J. Atulasimha, Appl. Phys. Lett. **109**, 102403 (2016).
[27]Y. Nii, T. Nakajima, A. Kikkawa, Y. Yamasaki, K. Ohishi, J. Suzuki, Y. Taguchi, T. Arima, Y. Tokura, and Y. Iwasa, Nat. Commun. **6**, 8539 (2015).
[28]S. Seki, Y. Okamura, K. Shibata, R. Takagi, N. D. Khanh, F. Kagawa, T. Arima, and Y. Tokura, Phys. Rev. B **96**, 220404 (2017).
[29]Y. Liu, N. Lei, W. Zhao, W. Liu, A. Ruotolo, H.-B. Braun, and Y. Zhou, Appl. Phys. Lett. **111**, 022406 (2017).
[30]Z. Li, Y. Zhang, Y. Huang, C. Wang, X. Zhang, Y. Liu, Y. Zhou, W. Kang, S. C. Koli, and N. Lei, J. Magn. Magn. Mater. **455**, 19 (2018).
[31]J.-M. Hu, T. Yang, and L.-Q. Chen, npj Comput. Mater. **4**, 62 (2018).
[32]COMSOL Multiphysics AB, *COMSOL Multiphysics User's Guide, 4.3 Version* (COMSOL Multiphysics AB, 2012).
[33]A. T. Hindmarch, A. W. Rushforth, R. P. Campion, C. H. Marrows, and B. L. Gallagher, Phys. Rev. B **83**, 212404 (2011).
[34]T. L. Gilbert, IEEE Trans. Magn. **40**, 3443 (2004).
[35]C.-Y. Liang, S. M. Keller, A. E. Sepulveda, A. Bur, W.-Y. Sun, K. Wetzlar, and G. P. Carman, Nanotechnology **25**, 435701 (2014).
[36]G. Consolo and G. Valenti, J. Appl. Phys. **121**, 043903 (2017).
[37]A. Vansteenkiste, J. Leliaert, M. Dvornik, M. Helsen, F. Garcia-Sanchez, and B. Van Waeyenberge, AIP Adv. **4**, 107133 (2014).
[38]M. Voto, L. Lopez-Diaz, and E. Martinez, Sci. Rep. **7**, 13559 (2017).
[39]L. Herrera Diez, F. García-Sánchez, J.-P. Adam, T. Devolder, S. Eimer, M. S. El Hadri, A. Lamperti, R. Mantovan, B. Ocker, and D. Ravelosona, Appl. Phys. Lett. **107**, 032401 (2015).
[40]W. Jiang, P. Upadhyaya, W. Zhang, G. Yu, M. B. Jungfleisch, F. Y. Fradin, J. E. Pearson, Y. Tserkovnyak, K. L. Wang, O. Heinonen, S. G. E. te Velthuis, and A. Hoffmann, Science **349**, 283 (2015).
[41]W. Jiang, X. Zhang, G. Yu, W. Zhang, X. Wang, M. Benjamin Jungfleisch, J. E. Pearson, X. Cheng, O. Heinonen, K. L. Wang, Y. Zhou, A. Hoffmann, and S. G. E. te Velthuis, Nat. Phys. **13**, 162 (2017).
[42]A. A. Thiele, Phys. Rev. Lett. **30**, 230 (1973).
[43]J. Iwasaki, M. Mochizuki, and N. Nagaosa, Nat. Nanotechnol. **8**, 742 (2013).
[44]V. Raposo, R. F. Luis Martinez, and E. Martinez, AIP Adv. **7**, 056017 (2017).
[45]C.-F. Pai, L. Liu, Y. Li, H. W. Tseng, D. C. Ralph, and R. A. Buhrman, Appl. Phys. Lett. **101**, 122404 (2012).
[46]R. Tomasello, E. Martinez, R. Zivieri, L. Torres, M. Carpentieri, and G. Finocchio, Sci. Rep. **4**, 6784 (2015).